INTERNATIONAL JOURNAL FOR NUMERICAL METHODS IN ENGINEERING
Int. J. Numer. Meth. Engng 2001; **50**:1017–1038

Finite element analysis of membrane wrinkling

K. Lu, M. Accorsi*,† and J. Leonard

Department of Civil and Environmental Engineering, University of Connecticut, 261 Glenbrook Rd. U-37, Storrs, CT 06269-2037, U.S.A.

SUMMARY

New results are presented for the finite element analysis of wrinkling in curved elastic membranes undergoing large deformation. Concise continuum level governing equations are derived in which singularities are eliminated. A simple and efficient algorithm with robust convergence properties is established to find the real strain and stress of the wrinkled membrane for Hookean materials. The continuum theory is implemented into a finite element code. Explicit formulas for the internal forces and the tangent stiffness matrix are derived. Numerical examples are presented that demonstrate the effectiveness of the new theory for predicting wrinkling in membranes undergoing large deformation. Copyright © 2001 John Wiley & Sons, Ltd.

KEY WORDS: membrane wrinkling; finite element method; parachutes

1. INTRODUCTION

Membranes are widely used as structural elements in many diverse engineering fields. Examples include parachutes, fabric structures, automobile airbags and human tissues. One difficulty in modelling membranes is to account for wrinkling phenomena that are not predicted by classical membrane theory.

Shells with low flexural stiffness can support a small amount of compressive stress before buckling. If such a shell is subjected to compression in one principal direction and tension in the other principal direction, it will buckle and many narrow wrinkles will form with crests and troughs roughly parallel to the tensile direction. As the flexural stiffness decreases, so do the critical buckling stress and the distance between the crests. When the flexural stiffness vanishes, so does the critical buckling stress and there would be an infinite number of infinitely narrow crests and troughs (wrinkles) exactly parallel to the tensile direction [1].

A membrane is essentially a thin shell with no flexural stiffness. Consequently, a membrane should not resist compression at all. It will be wrinkled or slack at the onset of any compressive

*Correspondence to: M. Accorsi, Department of Civil and Environmental Engineering, University of Connecticut, 261 Glenbrook Rd. U-37, Storrs, CT 06269-2037, U.S.A.
†E-mail: accorsi@engr.uconn.edu

Contract/grant sponsor: US Army Research Office; Contract/grant number: DAA04-96-1-0051
Contract/grant sponsor: US Army Natick RD & E center

Received 12 October 1999
Revised 5 April 2000

stress. However, in conventional membrane theory, the membrane can resist compression without wrinkling although its flexural stiffness vanishes.

At any point on its surface, a membrane must be in one of three states. In a 'slack' state, the membrane is not stretched in any direction. In a 'taut' state, the membrane is in tension in all directions. If the membrane is neither taut nor slack, it is in a 'wrinkled' state corresponding to uniaxial tension. There are, theoretically, an infinite number of fine wrinkles with crests and troughs along the tensile direction.

In a slack or wrinkled region, the real configuration of the membrane is undefined. To avoid this indefiniteness, the slack or wrinkled region can be replaced with a smoothed pseudo-surface where material points on the real wrinkled surface are projected onto the pseudo-surface. The pseudo-surface provides an average sense of the membrane configuration in the slack and wrinkled regions.

Wrinkling models in membranes have been studied extensively. In one approach, the constitutive relation of the membrane is modified to simulate wrinkling (e.g. References [2, 3]). However, the material properties of the membrane do not change when wrinkling occurs. Therefore, this approach is not consistent with the mechanics of membrane wrinkling. To date, this approach has been limited to isotropic materials.

A second approach is based on modifying the deformation tensor without changing the constitutive relation. Wu and Canfield [4] modified the deformation tensor by introducing an extra parameter. Roddeman *et al.* [5–7] generalized this approach to include anisotropic materials and determined the criterion to judge the state of the membrane at a point. Their theory was implemented using the finite element method to simulate wrinkled membranes. Due to the complexity of the formulation, explicit expressions for the internal forces and the tangent stiffness matrix were not derived. Internal forces were obtained numerically by simulating the virtual change of the element internal energy. The tangent stiffness matrix follows from numerical differentiation of the internal forces. Kang and Im [8] presented a new scheme to find the wrinkling direction which is consistent with the theory of Roddeman *et al.* In their scheme, Muller's method [9] is used to search for multiple roots of non-linear equations to find the wrinkling direction. Muttin [10] has generalized the wrinkling theory of Roddeman *et al.* for curved membranes using curvilinear co-ordinates and uses numerical differentiation to calculate the internal force and tangent stiffness matrix. To date, explicit expressions for the internal forces and the tangent stiffness matrix have not been presented.

In the present paper, the wrinkling theory of Roddeman *et al.* is formulated using curvilinear co-ordinates and a robust scheme to find the wrinkling direction is derived in which a single root is determined using Brent's method [9]. Concise explicit formulas for the internal forces and the tangent stiffness matrix are derived and implemented into a finite element code for modelling non-linear behaviour of tension structures [11]. This code is currently being developed to simulate the dynamic behaviour of parachutes [12]. Several numerical examples of classical wrinkling problems are presented to demonstrate the method. Finally, the wrinkling theory is used to simulate the inflation of a parachute from a highly folded initial configuration.

2. THEORY

2.1. Background

Tensor notation is used throughout this paper [13]. Greek indices take on the values 1 and 2 on the surface, and lower-case Latin indices take on the values 1, 2 and 3 in Euclidean space.

A repeated index indicates summation over the range of the index. Consider a membrane represented by its mid-surface in a plane–stress state. Let Ω_0 denote the reference surface which is assumed unstressed. Let Ω denote the current surface with slack and wrinkled regions replaced by pseudo-surfaces.

Assume the membrane moves in a three-dimensional Euclidean space. A convected curvilinear coordinate system (ξ^1, ξ^2) is attached to the mid-surface in taut regions or the pseudo-surface in wrinkled or slack regions.

The covariant base vectors of the convected coordinate system on Ω_0 and Ω are defined, respectively, as

$$\mathbf{G}_\alpha \equiv \frac{\partial \mathbf{X}}{\partial \xi^\alpha}, \quad \mathbf{g}_\alpha \equiv \frac{\partial \mathbf{x}}{\partial \xi^\alpha} \tag{1}$$

where $\mathbf{X}$ and $\mathbf{x}$ are position vectors of a particle referred to origins on Ω_0 and Ω, respectively. The covariant components of the metric tensor on Ω_0 and Ω are defined, respectively, as

$$G_{\alpha\beta} \equiv \mathbf{G}_\alpha \cdot \mathbf{G}_\beta, \quad g_{\alpha\beta} \equiv \mathbf{g}_\alpha \cdot \mathbf{g}_\beta \tag{2}$$

with their determinants as

$$G \equiv |G_{\alpha\beta}|, \quad g \equiv |g_{\alpha\beta}| \tag{3}$$

The construction of the convected co-ordinate system assures that G does not vanish on Ω_0. The contravariant components of metric tensors on Ω_0 are obtained from

$$\left[G^{\alpha\beta}\right] = \left[G_{\alpha\beta}\right]^{-1} \tag{4}$$

and the contravariant base vectors on Ω_0 are obtained from

$$\mathbf{G}^\alpha = G^{\alpha\beta}\mathbf{G}_\beta \tag{5}$$

Note that

$$\mathbf{G}_\beta \cdot \mathbf{G}^\alpha = \delta^\alpha_\beta, \quad \mathbf{g}_\beta \cdot \mathbf{g}^\alpha = \delta^\alpha_\beta \tag{6}$$

In a slack or wrinkled region of Ω, the quantities measured on the pseudo-surface are called 'nominal' ones while the quantities measured on the undefined real surface are called 'real' ones. In a taut region, these two classes of quantities are equivalent. The nominal deformation gradient tensor $\mathbf{F}$ is

$$\mathbf{F} \equiv \mathbf{g}_\alpha \mathbf{G}^\alpha \tag{7}$$

The nominal Green strain tensor $\mathbf{E}$ on Ω_0 is obtained from

$$\mathbf{E} = \tfrac{1}{2}(\mathbf{F}^{\mathrm{T}} \cdot \mathbf{F} - \mathbf{I}) = E_{\alpha\beta}\mathbf{G}^\alpha\mathbf{G}^\beta, \quad E_{\alpha\beta} = \tfrac{1}{2}(g_{\alpha\beta} - G_{\alpha\beta}) \tag{8}$$

where $\mathbf{I}$ is the unit tensor. The nominal second Piola–Kirchhoff stress $\mathbf{S}$ is determined from the constitutive relation

$$\mathbf{S} = \mathbf{H}(\mathbf{E}) \tag{9}$$

where $\mathbf{H}$ is a tensor function of $\mathbf{E}$ and

$$\mathbf{S} = S^{\alpha\beta}\mathbf{G}_\alpha\mathbf{G}_\beta \tag{10}$$

Here the membrane material is assumed to be elastic. The nominal Cauchy stress $\boldsymbol{\sigma}$ is obtained from

$$\boldsymbol{\sigma} = J^{-1}\mathbf{F}\cdot\mathbf{S}\cdot\mathbf{F}^{\mathrm{T}} = \sigma^{\alpha\beta}\mathbf{g}_{\alpha}\mathbf{g}_{\beta}, \quad \sigma^{\alpha\beta} = J^{-1}S^{\alpha\beta} \tag{11}$$

where J is the nominal Jacobian and

$$J = \det(\mathbf{F}) = \sqrt{\det(\mathbf{F}^{\mathrm{T}}\mathbf{F})} = \sqrt{G^{-1}g} \tag{12}$$

2.2. Slack state

The membrane is slack at a point on Ω if and only if it is not stretched in any direction, i.e.

$$\mathbf{a}\cdot\mathbf{E}\cdot\mathbf{a} \leqslant 0 \quad \text{or} \quad a^{\xi}a^{\eta}E_{\xi\eta} \leqslant 0 \tag{13}$$

where $\mathbf{a}$ is an arbitrary non-zero vector tangent to Ω_0. Let

$$a^1 = r_1 \cos\theta, \quad a^2 = r_1 \sin\theta, \quad r_1 \neq 0 \tag{14}$$

Substituting (14) into (13), we have

$$\frac{E_{11}+E_{22}}{2} + \frac{E_{11}-E_{22}}{2}\cos 2\theta + E_{12}\sin 2\theta \leqslant 0, \quad \forall\theta \tag{15}$$

Using a generalized Mohr's circle [13], the following condition is obtained for a point on Ω to be slack:

$$E_{11}+E_{22} \leqslant 0 \quad \text{and} \quad E_{11}E_{22} - E_{12}E_{12} \geqslant 0 \tag{16}$$

In a slack region, the real strain and stress both vanish.

2.3. Taut state

The membrane is taut at a point on Ω if and only if it is in tension in any direction, i.e.

$$\mathbf{b}\cdot\boldsymbol{\sigma}\cdot\mathbf{b} \geqslant 0 \tag{17}$$

where $\mathbf{b}$ is an arbitrary nonzero vector tangent to Ω. Substituting (11) into (17), one obtains

$$\hat{\mathbf{b}}\cdot\mathbf{S}\cdot\hat{\mathbf{b}} \geqslant 0 \quad \text{or} \quad b_{\alpha}b_{\beta}S^{\alpha\beta} \geqslant 0 \tag{18}$$

where $\hat{\mathbf{b}} = \mathbf{b}\cdot\mathbf{F}$ which is tangent to Ω_0. Using a generalized Mohr's circle [13], the following condition is obtained for a point on Ω to be taut:

$$S^{11}+S^{22} \geqslant 0 \quad \text{and} \quad S^{11}S^{22} - S^{12}S^{12} \geqslant 0 \tag{19}$$

In a taut region, the real strain and stress are the same as the nominal ones. Conventional membrane theory is applicable in this case.

2.4. Wrinkled state

If the membrane is neither slack nor taut at a point on Ω, it must be wrinkled. This is a uniaxial tension state in which one principal Cauchy stress is tensile and the other vanishes. Let $\mathbf{t}$ denote a unit vector in the tensile principal direction and $\mathbf{w}$ a unit vector in the other principal direction

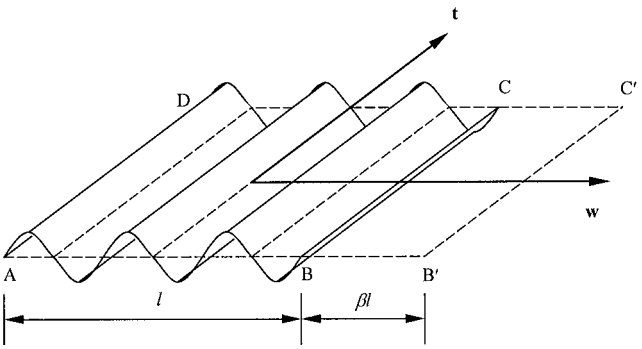

Figure 1. Wrinkled, pseudo and lengthened surfaces.

with zero principal stress. **t** and **w** also represent the direction along and transverse to the wrinkles, respectively. It follows that

$$\mathbf{w} = w_\alpha \mathbf{g}^\alpha, \quad \mathbf{w} \cdot \mathbf{w} = 1 \tag{20}$$

$$\mathbf{t} = t_\alpha \mathbf{g}^\alpha = t^\alpha \mathbf{g}_\alpha, \quad \mathbf{t} \cdot \mathbf{t} = 1 \tag{21}$$

$$\mathbf{t} \cdot \mathbf{w} = t^\alpha w_\alpha = 0 \tag{22}$$

The wrinkling algorithm is based on the observation that if the wrinkled membrane at a point on Ω is lengthened transverse to the wrinkles, the membrane will undergo rigid body movement until the wrinkles vanish. During the rigid body movement, the Green strain does not change while the Cauchy stress undergo the same rigid body movement with the membrane. Consequently, when the wrinkles just vanish, the lengthened surface will still be in a uniaxial tension state with the same principal stresses and directions. In Figure 1, the curved surface ABCD represents the wrinkled surface around a point on Ω, the plane ABCD represents the pseudo-surface and the plane AB′C′D represents the lengthened surface. When the wrinkles just vanish, the deformation gradient tensor $\tilde{\mathbf{F}}$ on the lengthened surface is given by [5]

$$\tilde{\mathbf{F}} = (\mathbf{I} + \beta \mathbf{w}\mathbf{w}) \cdot \mathbf{F} \tag{23}$$

where β is the ratio of lengthening which is also a measure of the amount of wrinkling. By definition,

$$\beta > 0 \tag{24}$$

The Green strain $\tilde{\mathbf{E}}$ on the undefined wrinkled surface, which equals the Green strain on the lengthened surface, is determined from

$$\tilde{\mathbf{E}} = \tfrac{1}{2}\left(\tilde{\mathbf{F}}^{\mathrm{T}} \cdot \tilde{\mathbf{F}} - \mathbf{I}\right) = \mathbf{E} + \tfrac{1}{2}\beta(2+\beta)\hat{\mathbf{w}}\hat{\mathbf{w}} \tag{25}$$

where

$$\tilde{\mathbf{E}} = \tilde{E}_{\alpha\beta}\mathbf{g}^\alpha \mathbf{g}^\beta, \quad \tilde{E}_{\alpha\beta} = E_{\alpha\beta} + \tfrac{1}{2}\beta(2+\beta)w_\alpha w_\beta, \quad \hat{\mathbf{w}} = \mathbf{w} \cdot \mathbf{F} = w_\alpha \mathbf{G}^\alpha \tag{26}$$

The second Piola–Kirchhoff stress $\tilde{\mathbf{S}}$ on the lengthened surface is determined from

$$\tilde{\mathbf{S}} = \mathbf{H}(\tilde{\mathbf{E}}) \tag{27}$$

where

$$\tilde{\mathbf{S}} = \tilde{S}^{\alpha\beta}\mathbf{G}_\alpha\mathbf{G}_\beta \tag{28}$$

The Cauchy stress $\tilde{\boldsymbol{\sigma}}$ on the lengthened surface can be calculated from

$$\tilde{\boldsymbol{\sigma}} = \tilde{J}^{-1}\tilde{\mathbf{F}}\cdot\tilde{\mathbf{S}}\cdot\tilde{\mathbf{F}}^{\mathrm{T}} \tag{29}$$

where

$$\tilde{J} = \det(\tilde{\mathbf{F}}) = \sqrt{\det(\tilde{\mathbf{F}}^{\mathrm{T}}\tilde{\mathbf{F}})} = \sqrt{\det(2\tilde{\mathbf{E}}+\mathbf{I})} = \sqrt{G^{-1}|2\tilde{E}_{\alpha\beta}+G_{\alpha\beta}|} > 0 \tag{30}$$

When the wrinkles just vanish, the lengthened surface is still in uniaxial tension, and $\tilde{\boldsymbol{\sigma}}$ satisfies the following conditions:

$$\tilde{\boldsymbol{\sigma}}\cdot\mathbf{w} = \mathbf{0} \tag{31}$$

$$\mathbf{t}\cdot\tilde{\boldsymbol{\sigma}}\cdot\mathbf{t} > 0 \tag{32}$$

Substituting (29) into (31) and (32) and noting that

$$\mathbf{w}\cdot\tilde{\mathbf{F}} = (1+\beta)\mathbf{w}\cdot\mathbf{F}, \quad \mathbf{t}\cdot\tilde{\mathbf{F}} = \mathbf{t}\cdot\mathbf{F} \tag{33}$$

one obtains the following conditions that are equivalent to (31) and (32):

$$\tilde{\mathbf{S}}\cdot\hat{\mathbf{w}} = \mathbf{0} \tag{34}$$

$$\hat{\mathbf{t}}\cdot\tilde{\mathbf{S}}\cdot\hat{\mathbf{t}} > 0 \tag{35}$$

where

$$\hat{\mathbf{t}} = \mathbf{t}\cdot\mathbf{F} = t_\alpha\mathbf{G}^\alpha \tag{36}$$

and the vectors $\hat{\mathbf{t}}$ and $\hat{\mathbf{w}}$ are tangent to Ω_0. Unlike $\mathbf{t}$ and $\mathbf{w}$, these vectors are not necessarily orthonormal but are still linearly independent. Equation (34) shows that $\hat{\mathbf{w}}$ is along the principal direction of $\tilde{\mathbf{S}}$ where the corresponding principal stress vanishes. Let $\mathbf{n}$ denote a unit vector in the other principal direction of $\tilde{\mathbf{S}}$. It follows that

$$\mathbf{n} = n^\alpha\mathbf{G}_\alpha, \quad \mathbf{n}\cdot\mathbf{n} = 1, \quad \mathbf{n}\cdot\hat{\mathbf{w}} = n^\alpha w_\alpha = 0 \tag{37}$$

and

$$\tilde{\mathbf{S}} = \tilde{S}_{\mathrm{I}}\mathbf{n}\mathbf{n} \tag{38}$$

where $\tilde{S}_{\mathrm{I}}$ is the principal stress of $\tilde{\mathbf{S}}$ along $\mathbf{n}$. The vector $\hat{\mathbf{t}}$ can be decomposed as

$$\hat{\mathbf{t}} = c_1\hat{\mathbf{w}} + c_2\mathbf{n}, \quad c_2 \neq 0 \tag{39}$$

Substituting (39) into (35), one obtains

$$\hat{\mathbf{t}}\cdot\tilde{\mathbf{S}}\cdot\hat{\mathbf{t}} = c_2^2\mathbf{n}\cdot\tilde{\mathbf{S}}\cdot\mathbf{n} = c_2^2\tilde{S}_{\mathrm{I}} \tag{40}$$

which means (35) is equivalent to

$$\tilde{S_{\mathrm{I}}} > 0 \tag{41}$$

For an elastic material, the fact that the strain energy should be positive requires

$$\tilde{\mathbf{S}} : \tilde{\mathbf{E}} > 0 \tag{42}$$

Since

$$\tilde{\mathbf{S}} : \tilde{\mathbf{E}} = (S_1 \mathbf{nn}) : [\mathbf{E} + \tfrac{1}{2}\beta(2+\beta)\hat{\mathbf{w}}\hat{\mathbf{w}}] = S_1 \mathbf{n} \cdot \mathbf{E} \cdot \mathbf{n} \tag{43}$$

Condition (41) is equivalent to

$$\mathbf{n} \cdot \mathbf{E} \cdot \mathbf{n} > 0 \tag{44}$$

Meanwhile, (34) is equivalent to

$$\hat{\mathbf{w}} \cdot \tilde{\mathbf{S}} \cdot \hat{\mathbf{w}} = 0 \tag{45}$$

$$\mathbf{v} \cdot \tilde{\mathbf{S}} \cdot \hat{\mathbf{w}} = 0 \tag{46}$$

where $\mathbf{v}$ is an arbitrary vector tangent to Ω_0 which is linearly independent of $\hat{\mathbf{w}}$.

In summary, for a wrinkled membrane, the following conditions apply:

$$\hat{\mathbf{w}} \cdot \tilde{\mathbf{S}} \cdot \hat{\mathbf{w}} = 0 \quad \text{or} \quad w_\alpha w_\beta \tilde{S}^{\alpha\beta} = 0 \tag{47}$$

$$\mathbf{v} \cdot \tilde{\mathbf{S}} \cdot \hat{\mathbf{w}} = 0 \quad \text{or} \quad v_\alpha w_\beta \tilde{S}^{\alpha\beta} = 0 \tag{48}$$

$$\mathbf{n} \cdot \mathbf{E} \cdot \mathbf{n} > 0 \quad \text{or} \quad n^\alpha n^\beta E_{\alpha\beta} > 0 \tag{49}$$

These conditions can be simplified by defining

$$\mathbf{s}_1 = \cos\,\theta, \quad \mathbf{s}_2 = \sin\,\theta, \quad \mathbf{s}_1' = -\sin\,\theta, \quad \mathbf{s}_2' = \cos\theta \tag{50}$$

$$w_1 = \alpha \mathbf{s}_1, \qquad w_2 = \alpha \mathbf{s}_2, \qquad \alpha \neq 0 \tag{51}$$

Using (37), one can determine n^α by

$$n^1 = r_2 \mathbf{s}_1', \quad n^2 = r_2 \mathbf{s}_2', \quad r_2 \neq 0 \tag{52}$$

Linear independence of w_α and v_α is satisfied by

$$v_1 = r_3 \mathbf{s}_1', \quad v_2 = r_3 \mathbf{s}_2', \quad r_3 \neq 0 \tag{53}$$

Substituting (51) into (26), one obtains

$$\tilde{E}_{\xi\eta} = E_{\xi\eta} + \gamma \mathbf{s}_\xi \mathbf{s}_\eta, \quad \gamma = \tfrac{1}{2}\alpha^2\beta(2+\beta) \tag{54}$$

The restriction of (24) is equivalent to

$$\gamma > 0 \tag{55}$$

Substituting (51)–(54) and (27) into (47)–(49), one obtains the following conditions for membrane wrinkling:

$$\mathbf{s}_\alpha \mathbf{s}_\beta \tilde{S}^{\alpha\beta} = 0 \tag{56}$$

$$\mathbf{s}'_\alpha \mathbf{s}_\beta \tilde{S}^{\alpha\beta} = 0 \tag{57}$$

$$\mathbf{s}'_\alpha \mathbf{s}'_\beta E_{\alpha\beta} > 0 \tag{58}$$

There are two equations, (56) and (57), with two unknowns, γ and θ, which also need to satisfy the inequality constraints (55) and (58).

2.5. *Wrinkling direction*

For a general elastic material, Equations (56) and (57) are coupled and non-linear. However, they can be uncoupled if the material obeys a generalized Hooke's law, i.e.

$$\mathbf{S} = \mathbf{C} : \mathbf{E}, \quad \tilde{\mathbf{S}} = \mathbf{C} : \tilde{\mathbf{E}}, \quad \mathbf{C} = C^{\alpha\beta\xi\eta} \mathbf{G}_\alpha \mathbf{G}_\beta \mathbf{G}_\xi \mathbf{G}_\eta \tag{59}$$

where $\mathbf{C}$ is the constant elasticity tensor. This constitutive equation is appropriate for membranes that undergo large displacement and large rotation but small strain. Substituting (59) and (54) into (56) and (57), one obtains

$$\mathbf{s}_\alpha \mathbf{s}_\beta S^{\alpha\beta} + \gamma \mathbf{s}_\alpha \mathbf{s}_\beta C^{\alpha\beta\xi\eta} \mathbf{s}_\xi \mathbf{s}_\eta = 0 \tag{60}$$

$$\mathbf{s}'_\alpha \mathbf{s}_\beta S^{\alpha\beta} + \gamma \mathbf{s}'_\alpha \mathbf{s}_\beta C^{\alpha\beta\xi\eta} \mathbf{s}_\xi \mathbf{s}_\eta = 0 \tag{61}$$

Solution of (60) for γ gives

$$\gamma = -\frac{\mathbf{s}_\xi \mathbf{s}_\eta S^{\xi\eta}}{\mathbf{s}_\sigma \mathbf{s}_\varsigma C^{\sigma\varsigma\tau\upsilon} \mathbf{s}_\tau \mathbf{s}_\upsilon} \tag{62}$$

Since the denominator is always positive, condition (55) is equivalent to

$$\mathbf{s}_\sigma \mathbf{s}_\varsigma S^{\sigma\varsigma} < 0 \tag{63}$$

Substituting (62) into (61), one obtains

$$f(\theta) = \mathbf{s}'_\alpha \mathbf{s}_\beta S^{\alpha\beta} - \frac{\mathbf{s}_\xi \mathbf{s}_\eta S^{\xi\eta}}{\mathbf{s}_\sigma \mathbf{s}_\varsigma C^{\sigma\varsigma\tau\upsilon} \mathbf{s}_\tau \mathbf{s}_\upsilon} \mathbf{s}'_\alpha \mathbf{s}_\beta C^{\alpha\beta\lambda\pi} \mathbf{s}_\lambda \mathbf{s}_\pi = 0 \tag{64}$$

This is a non-linear equation for one unknown variable, θ.

Notice that the set of θ that satisfies the two inequalities, (58) and (63), can be found before solving for θ with (64). This is why (49) is preferable to (35). Since neither (13) nor (18) is true for a wrinkled membrane, there must be some range of θ where both (58) and (63) are true. This is consistent with the criterion used to judge the wrinkling state. Expanding the first inequality (58) and utilizing trigonometric relations, one obtains

$$\frac{E_{11} + E_{22}}{2} + \left(\frac{E_{22} - E_{11}}{2} \right) \cos 2\theta - E_{12} \sin 2\theta > 0 \tag{65}$$

From a generalized Mohr's circle, the solution of inequality (58) is

$$\left\{\theta : \theta_1^E - \theta_0^E + 2k\pi < 2\theta < \theta_2^E - \theta_0^E + 2k\pi,\ k \in \mathbb{Z}\right\} \tag{66}$$

where $\mathbb{Z}$ denote the set of all integers,

$$\begin{aligned} &\cos\theta_0^E = \frac{E_{22} - E_{11}}{2R_E} \qquad \cos\theta_1^E = -\frac{E_{11} + E_{22}}{2R_E} \qquad \cos\theta_2^E = -\frac{E_{11} + E_{22}}{2R_E} \\ &\sin\theta_0^E = \frac{E_{12}}{R_E} \qquad \sin\theta_1^E = -\frac{\sqrt{E_{12}E_{12} - E_{11}E_{22}}}{R_E} \qquad \sin\theta_2^E = \frac{\sqrt{E_{12}E_{12} - E_{11}E_{22}}}{R_E} \end{aligned} \tag{67}$$

and

$$R_E = \sqrt{\left(\frac{E_{11} - E_{22}}{2}\right)^2 + E_{12}E_{12}} \tag{68}$$

The angles, θ_0^E, θ_1^E and θ_2^E, are uniquely determined on $[-\pi, \pi]$.

Similarly, expanding (63) and utilizing trigonometric relations, one obtains

$$\frac{S^{11} + S^{22}}{2} + \frac{S^{11} - S^{22}}{2}\cos 2\theta + S^{12}\sin 2\theta < 0 \tag{69}$$

From a generalized Mohr's circle, the solution of inequality (63) is

$$\left\{\theta : \theta_1^S - \theta_0^S + 2k\pi < 2\theta < \theta_2^S - \theta_0^S + 2(k+1)\pi,\ k \in \mathbb{Z}\right\} \tag{70}$$

where

$$\begin{aligned} &\cos\theta_0^S = \frac{S^{11} - S^{22}}{R_S} \qquad \cos\theta_1^S = -\frac{S^{11} + S^{22}}{2R_S} \qquad \cos\theta_2^S = -\frac{S^{11} + S^{22}}{2R_S} \\ &\sin\theta_0^S = -\frac{S^{12}}{R_S} \qquad \sin\theta_1^S = \frac{\sqrt{S^{12}S^{12} - S^{11}S^{22}}}{R_S} \qquad \sin\theta_2^S = -\frac{\sqrt{S^{12}S^{12} - S^{11}S^{22}}}{R_S} \end{aligned} \tag{71}$$

and

$$R_S = \sqrt{\left(\frac{S^{11} - S^{22}}{2}\right)^2 + S^{12}S^{12}} \tag{72}$$

The angles, θ_0^S, θ_1^S and θ_2^S, are uniquely determined on $[0, 2\pi]$.

Note that one need only find the solution of θ within a half-cycle. Let that half-cycle be $\left\{\theta : -\pi - \theta_0^E \leqslant 2\theta < \pi - \theta_0^E\right\}$. Let Q_E and Q_S denote the θ of (66) and (70) within that half-cycle, respectively. Q_E should be

$$Q_E = \left\{\theta : \theta_1^E - \theta_0^E < 2\theta < \theta_2^E - \theta_0^E\right\} \tag{73}$$

The set in (70) can be rewritten as

$$\left\{\theta : \left(\theta_1^S - \theta_0^S + \theta_0^E + \pi + 2k\pi\right) - \pi - \theta_0^E < 2\theta < \left(\theta_2^S - \theta_0^S + \theta_0^E + 3\pi + 2k\pi\right) - \pi - \theta_0^E,\ k \in \mathbb{Z}\right\} \tag{74}$$

Let

$$\theta_1 = \left(\theta_1^S - \theta_0^S + \theta_0^E + \pi\right) \bmod 2\pi, \quad \theta_2 = \left(\theta_2^S - \theta_0^S + \theta_0^E + \pi\right) \bmod 2\pi \tag{75}$$

where $0 \leqslant \theta_1, \theta_2 < 2\pi$. Q_S should be

$$Q_S = \begin{cases} \{\theta : \theta_1 - \pi - \theta_0^E < 2\theta < \theta_2 - \pi - \theta_0^E\} & \text{if } \theta_1 < \theta_2 \\ \{\theta : \theta_1 - \pi - \theta_0^E < 2\theta < \pi - \theta_0^E \text{ or } -\pi - \theta_0^E \leqslant 2\theta < \theta_2 - \pi - \theta_0^E\} & \text{if } \theta_1 > \theta_2 \end{cases} \tag{76}$$

Within $Q_E \cap Q_S$, Equation (64) must have a unique root of θ. $Q_E \cap Q_S$ may consist of one or two intervals. In the case of two intervals, we have to determine in which interval the unique root exists. Suppose one interval is (a, b). If $f(a) f(b) < 0$, the root must be in this interval. If $f(a) f(b) > 0$, the root must be in the other interval. The unique root within the known interval can be found by Brent's method [9]. Brent's method is guaranteed to converge so long as the function can be evaluated within the initial interval known to contain a root.

2.6. Wrinkling stress

After θ is determined, one can obtain $\tilde{\mathbf{S}}$ and $\tilde{\mathbf{E}}$. To obtain $\tilde{\boldsymbol{\sigma}}$ from the above results, first note that

$$\tilde{\boldsymbol{\sigma}} = \tilde{\sigma}_1 \mathbf{t}\mathbf{t} \tag{77}$$

From (21), (22) and (51), we have

$$\mathbf{t} = t^\alpha \mathbf{g}_\alpha, \quad t^1 = \mathbf{s}_1' \Big/ \sqrt{g_{\alpha\beta}\mathbf{s}_\alpha'\mathbf{s}_\beta'}, \quad t^2 = \mathbf{s}_2' \Big/ \sqrt{g_{\alpha\beta}\mathbf{s}_\alpha'\mathbf{s}_\beta'} \tag{78}$$

The non-zero principal stress along $\mathbf{t}$ is

$$\tilde{\boldsymbol{\sigma}}_1 = \mathbf{t} \cdot \tilde{\boldsymbol{\sigma}} \cdot \mathbf{t} = \tilde{J}^{-1} \hat{\mathbf{t}} \cdot \tilde{\mathbf{S}} \cdot \hat{\mathbf{t}} = \tilde{J}^{-1} g_{\alpha\xi} t^\xi g_{\beta\eta} t^\eta \tilde{S}^{\alpha\beta} = (g_{\sigma\tau}\mathbf{s}_\sigma'\mathbf{s}_\tau'\tilde{J})^{-1} g_{\alpha\xi}\mathbf{s}_\xi' g_{\beta\eta}\mathbf{s}_\eta' \tilde{S}^{\alpha\beta} \tag{79}$$

Note that $\tilde{\boldsymbol{\sigma}}$ is not measured on the pseudo-surface, but on the lengthened surface. It is the same as the stress on the undefined wrinkled surface except for some rigid body movement.

Remark 1. Equation (13) means that the matrix $[-E_{\alpha\beta}]$ is positive definite. Condition (16) can also be derived from the requirement of a positive-definite matrix. This is also true for (18) and (19).

Remark 2. The covariant base vectors $\mathbf{g}_\alpha$ on Ω may be linearly dependent. In that case, the contravariant base vectors $\mathbf{g}^\alpha$ in (20) and (21) are undefined. However, the governing equations (56) to (58) for wrinkled membrane are still valid. The singularities have been eliminated in those equations.

3. FINITE ELEMENT IMPLEMENTATION

3.1. Geometry of membrane elements

A total Lagrangian formulation and a displacement-based isoparametric finite element formulation are adopted here. Assume there exists a fixed Cartesian co-ordinate system with orthonormal base vectors $\mathbf{e}_i$ in the Euclidean space. Consider a membrane element with natural co-ordinate system (ξ^1, ξ^2) act as the convected co-ordinate system. The co-ordinate interpolations on Ω_0 and Ω and the displacement interpolation are

$$\mathbf{X} = \sum_{I=1}^{q} h^I \mathbf{X}^I, \quad \mathbf{x} = \sum_{I=1}^{q} h^I \mathbf{x}^I, \quad \mathbf{u} = \sum_{I=1}^{q} h^I \mathbf{u}^I \tag{80}$$

where h^I is the interpolation function for the Ith node and q is the total number of nodes of the element. The covariant base vectors of the natural co-ordinate system on Ω_0 and Ω are

$$\mathbf{G}_\alpha = \sum_{I=1}^{q} h^I_{,\alpha}\mathbf{X}^I, \quad \mathbf{g}_\alpha = \sum_{I=1}^{q} h^I_{,\alpha}\mathbf{x}^I \tag{81}$$

where

$$h^I_{,\alpha} \equiv \frac{\partial h^I}{\partial \xi^\alpha} \tag{82}$$

With these basic quantities known at any point on the element, the state (i.e. taut, slack, or wrinkled) and the real strain and stress can be obtained using the theory in Section 2.

3.2. Internal forces and tangent stiffness matrix of membrane element

From the principle of virtual work, the internal forces equivalent to the stress on the element is determined from

$$T^I_i = \int_{\Omega_0} S^{\alpha\beta}\frac{\partial E_{\alpha\beta}}{\partial u^I_i}\,\mathrm{d}A \tag{83}$$

where

$$u^I_i = \mathbf{u}^I \cdot \mathbf{e}_i, \quad T^I_i = \mathbf{T}^I \cdot \mathbf{e}_i \tag{84}$$

and $\mathbf{u}^I$ and $\mathbf{T}^I$ are displacement vector and internal force vector on Ith node of the element.

The coefficient $K_{u^I_i u^J_j}$ of the tangent stiffness matrix corresponds to displacements, u^I_i and u^J_j, and is determined from

$$K_{u^I_i u^J_j} = \int_{\Omega_0}\left(C^{\xi\eta\alpha\beta}\frac{\partial E_{\xi\eta}}{\partial u^J_j}\frac{\partial E_{\alpha\beta}}{\partial u^I_i} + S^{\alpha\beta}\frac{\partial^2 E_{\alpha\beta}}{\partial u^I_i\,\partial u^J_j}\right)\mathrm{d}A \tag{85}$$

where

$$C^{\alpha\beta\xi\eta} \equiv \frac{\partial S^{\alpha\beta}}{\partial E_{\xi\eta}} \tag{86}$$

For a material that obeys a generalized Hooke's law, $C^{\alpha\beta\xi\eta}$ equals the constant elasticity tensor.

The stress and strain used in (83) and (85) should be the real values on the undefined wrinkled or slack surface. For a slack membrane, the real strain and the real stress vanish as does the partial derivative of the real strain with respect to the nodal displacements. Therefore, at a slack point in a membrane element, the contribution to the internal force vector and the tangent stiffness matrix are zero.

For a taut or wrinkled point in a membrane element, note that

$$\mathbf{x} = \mathbf{X} + \mathbf{u} \tag{87}$$

where **u** is the displacement vector. Since Ω_0 does not change with the motion of the element, it follows that

$$\frac{\partial \mathbf{x}^J}{\partial u_i^I} = \frac{\partial \mathbf{u}^J}{\partial u_i^I} = \frac{\partial u_k^J}{\partial u_i^I}\mathbf{e}_k = \delta_{IJ}\delta_{ki}\mathbf{e}_k = \delta_{IJ}\mathbf{e}_i \tag{88}$$

$$\frac{\partial^2 \mathbf{x}^K}{\partial u_i^I\, \partial u_j^J} = \frac{\partial^2 \mathbf{u}^K}{\partial u_i^I\, \partial u_j^J} = \frac{\partial}{\partial u_j^{(J)}}\left(\frac{\partial \mathbf{u}^K}{\partial u_i^I}\right) = \frac{\partial}{\partial u_j^J}(\delta_{KI}\mathbf{e}_i) = \mathbf{0} \tag{89}$$

$$\frac{\partial \mathbf{g}_\alpha}{\partial u_i^I} = \sum_{J=1}^{q} h_{,\alpha}^J \frac{\partial \mathbf{x}^J}{\partial u_i^I} = h_{,\alpha}^I \mathbf{e}_i \tag{90}$$

$$\frac{\partial g_{\alpha\beta}}{\partial u_i^I} = \frac{\partial \mathbf{g}_\alpha}{\partial u_i^I}\cdot \mathbf{g}_\beta + \mathbf{g}_\alpha \cdot \frac{\partial \mathbf{g}_\beta}{\partial u_i^I} = \sum_{J=1}^{q} (h_{,\alpha}^I h_{,\beta}^J + h_{,\alpha}^J h_{,\beta}^I) x_i^J \tag{91}$$

$$\frac{\partial^2 \mathbf{g}_\alpha}{\partial u_i^I\, \partial u_j^J} = \sum_{K=1}^{q} h_{,\alpha}^{(J)} \frac{\partial^2 \mathbf{x}^K}{\partial u_i^I\, \partial u_j^J} = \mathbf{0} \tag{92}$$

$$\begin{aligned}\frac{\partial^2 g_{\alpha\beta}}{\partial u_i^I\, \partial u_j^J} &= \frac{\partial^2 \mathbf{g}_\alpha}{\partial u_i^I\, \partial u_j^J}\cdot \mathbf{g}_\beta + \frac{\partial \mathbf{g}_\alpha}{\partial u_i^I}\cdot \frac{\partial \mathbf{g}_\beta}{\partial u_j^J} + \frac{\partial \mathbf{g}_\alpha}{\partial u_j^J}\cdot \frac{\partial \mathbf{g}_\beta}{\partial u_i^I} + \mathbf{g}_\alpha \cdot \frac{\partial^2 \mathbf{g}_\beta}{\partial u_i^I\, \partial u_j^J} \\ &= \left(h_{,\alpha}^I h_{,\beta}^J + h_{,\beta}^I h_{,\alpha}^J\right)\delta_{ij}\end{aligned} \tag{93}$$

$$\frac{\partial E_{\alpha\beta}}{\partial u_i^I} = \frac{1}{2}\frac{\partial g_{\alpha\beta}}{\partial u_i^I}, \quad \frac{\partial^2 E_{\alpha\beta}}{\partial u_i^I\, \partial u_j^J} = \frac{1}{2}\frac{\partial^2 g_{\alpha\beta}}{\partial u_i^I\, \partial u_j^J} \tag{94}$$

If the membrane is taut at a point, (88)–(94) provide the partial derivative of the real strain with respect to the nodal displacements needed to calculate the internal force vector and the tangent stiffness matrix. If the membrane is wrinkled at a point, the real strain $\tilde{E}_{\xi\eta}$ and the real stress $\tilde{S}^{\alpha\beta}$, must be used. To obtain $\partial \tilde{E}_{\alpha\beta}/\partial u_i^I$ and $\partial^2 \tilde{E}_{\alpha\beta}/\left(\partial u_i^I\, \partial u_j^J\right)$, partial derivatives of the wrinkling equation (64) with respect to the nodal displacements are performed. The resulting equation can be written in the following form:

$$\frac{\partial \theta}{\partial u_i^I} P + Q_1 = 0 \tag{95}$$

which is solved for $\partial\theta/\partial u_i^I$. From this result, $\partial \tilde{E}_{\alpha\beta}/\partial u_i^I$ can be obtained (see the appendix).

To obtain $\partial^2 \tilde{E}_{\alpha\beta}/(\partial u_i^I\, \partial u_j^J)$, the second partial derivative of the wrinkling equation (64) with respect to the nodal displacements is taken. The resulting equation can be written in the following form:

$$\frac{\partial^2 \theta}{\partial u_i^I\, \partial u_j^J} P + Q_2 = 0 \tag{96}$$

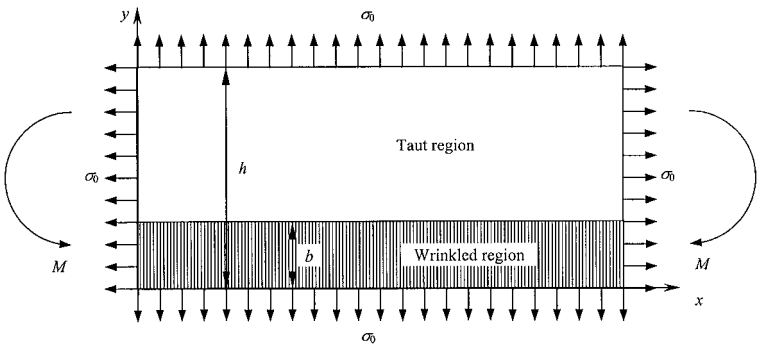

Figure 2. Beam-like membrane.

which is solved for $\partial^2\theta/(\partial u_i^I\,\partial u_j^J)$. From this result, $\partial^2\tilde{E}_{\alpha\beta}/(\partial u_i^I\,\partial u_j^J)$ can be obtained (see the appendix).

In practice, the internal forces and the tangent stiffness matrix for each element are obtained by Gauss numerical integration where the state of each integration point is evaluated and the appropriate relations from above are then used. The element equations are assembled to obtain the global internal forces and the tangent stiffness matrix. The non-linear dynamic incremental response to both conservative and non-conservative (pressure) loadings are iteratively integrated in time using an implicit Newmark method. In each time increment, Newton–Raphson method is adopted to solve the global non-linear equations.

Remark 3. If we want to obtain the partial derivative of strain for general elastic material, we need to take the partial derivatives of (56) and (57) with respect to the nodal displacement and then solve the equations for partial derivatives of γ and θ.

4. NUMERICAL EXAMPLES

4.1. Pure bending of a pretensioned beam-like membrane

Consider a beam-like rectangular plane membrane shown in Figure 2 [2]. The width and thickness are h and t, respectively. The membrane is tensioned by a uniform normal stress σ_0 in both x- and y-direction and subject to an in-plane bending moment M applied on its two ends. As M is increased, a band of vertical wrinkles with height b appears along the compressed edge. The height b is given by

$$\frac{b}{h}=\begin{cases} 0, & \dfrac{M}{Ph}<\dfrac{1}{6} \\ \dfrac{3M}{Ph}-\dfrac{1}{2}, & \dfrac{1}{6}\leqslant\dfrac{M}{Ph}<\dfrac{1}{2} \end{cases} \tag{97}$$

The stress within the membrane may be expressed as

$$\frac{\sigma_x}{\sigma_0} = \begin{cases} 2\left(\frac{y}{h} - \frac{b}{h}\right) \Big/ \left(1 - \frac{b}{h}\right)^2, & \frac{b}{h} < \frac{y}{h} \leqslant 1 \\ 0, & 0 \leqslant \frac{y}{h} \leqslant \frac{b}{h} \end{cases} \tag{98}$$

$$\frac{\sigma_y}{\sigma_0} = 1 \tag{99}$$

$$\tau_{xy} = 0 \tag{100}$$

Let κ denote the overall curvature of the membrane acting as a beam. The relation between M and κ is given by

$$\frac{2M}{Ph} = \begin{cases} \frac{1}{3}\frac{Eth^2}{2P}\kappa, & \frac{Eth^2}{2P}\kappa \leqslant 1 \\ 1 - \frac{2}{3}\sqrt{\frac{2P}{Eth^2\kappa}}, & \frac{Eth^2}{2P}\kappa > 1 \end{cases} \tag{101}$$

where E is the Young's modulus of the membrane material.

A uniform mesh consisting of five rows and 10 columns of nine-node isoparametric elements was used. The load on the right end is replaced by two concentrated loads whose effect is equivalent to M and the tension σ_0 in the x-direction. The curvature of the finite element model is computed from the nodal displacements by assuming that the y-displacements are parabolic in the x-direction for a beam in pure bending. A comparison of the numerical and analytical curvature as a function of applied moment is shown in Figure 3. The stresses on the section are sampled in the middle of the beam. By Saint-Venant's principle, the local effect of the concentrated load on the right end can be ignored there. A comparison of the numerical and analytical stresses across the beam height for various values of M is shown in Figure 4. All these results agree very well over a wide range of the values of M.

4.2. Torsion of a membrane

A circular annulus-shaped membrane is attached to a rigid disk at the inner edge and to a guard ring at the outer edge [7]. Turning the rigid disk causes wrinkling of the membrane. The rigid disk is rotated over 10°. The inner radius of the membrane is 5 m and the outer radius 12.5 m. Thickness of membrane is 1.0 m. Linear orthotropic material behaviour is assumed, i.e.

$$\begin{bmatrix} S_{11} \\ S_{22} \\ S_{12} \end{bmatrix} = \mathbf{D}^{-1} \begin{bmatrix} E_{11} \\ E_{22} \\ E_{12} \end{bmatrix} \tag{102}$$

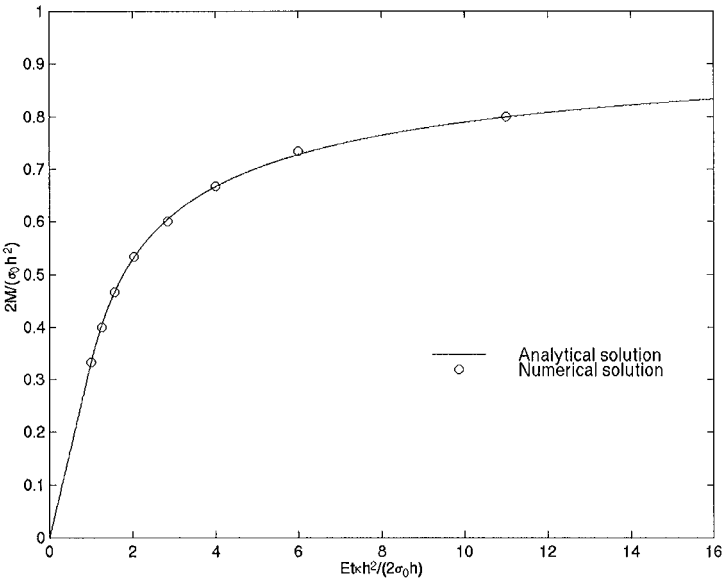

Figure 3. Bending moment vs curvature.

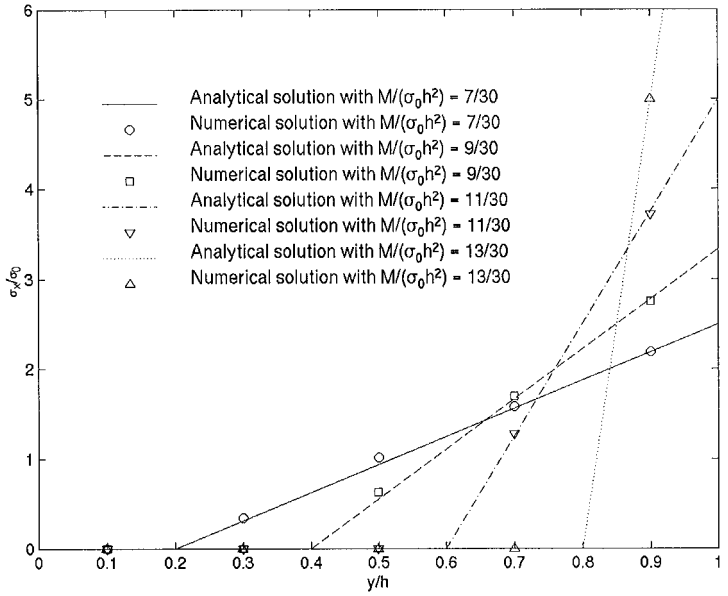

Figure 4. Cauchy stress on the section.

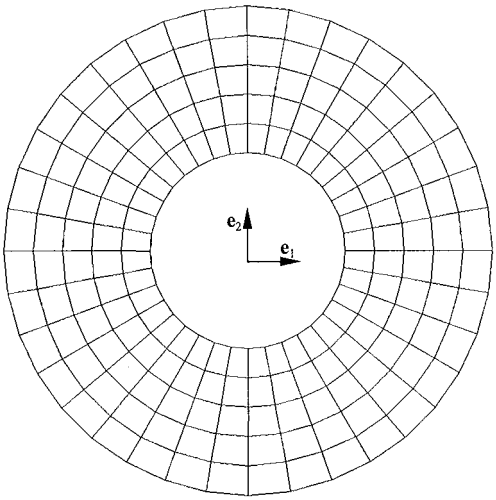

Figure 5. Initial finite element mesh of the membrane.

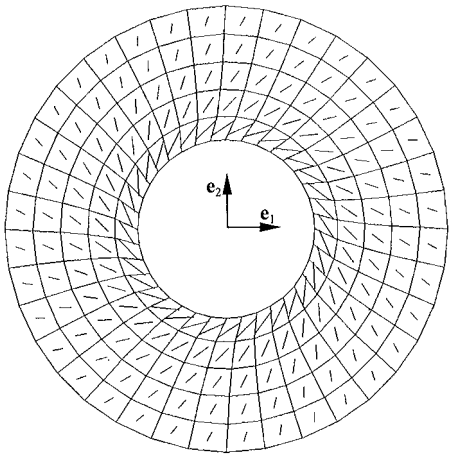

Figure 6. Deformed mesh with principal Cauchy stresses vectors for isotropic analysis.

where

$$\mathbf{D} = \begin{bmatrix} \dfrac{1}{E_1} & -\dfrac{v_{21}}{E_2} & 0 \\ -\dfrac{v_{12}}{E_2} & \dfrac{1}{E_2} & 0 \\ 0 & 0 & \dfrac{1}{2G} \end{bmatrix} \tag{103}$$

For isotropic material property, the material constants are: $E_1 = E_2 = E = 10^5$ Pa, $v_{12} = v_{21} = v = 0.3$, $G = E/2(1+v)$. For orthotropic material property, material property constants are: $E_1 = 10^5$ Pa, $E_2 = 10^6$ Pa, $v_{12} = 0.3$, $E_1 v_{12} = E_2 v_{21}$, $G = 0.385 \times 10^5$ Pa. The finite element mesh for the initial configuration is shown in Figure 5. The deformed shapes are shown in Figures 6 and 7 for isotropic and orthotropic material properties, respectively. The vectors in the centre of each element represent the magnitude of the principal stresses. Since all the elements are wrinkled, only one vector appears on each element that represents the non-zero tensile principal stress. The maximum tensile stress in Figure 6 is on the inner edge with a value of 2.6×10^4 Pa. These figures and values agree well with previously published results [7].

4.3. Inflation of a square airbag

Two square membranes are joined along their perimeters and are inflated by internal pressure [14]. The pressure is $0.5\,\text{lb/ft}^2$. The side length of the airbag $L = 1$ ft, and thickness of the membrane is 0.0001 ft. The Young's modulus is $4.32 \times 10^6\,\text{lb/ft}^2$ and the Poisson ratio 0.3. Utilizing symmetry, only one-eighth of the airbag (ABCD) is modelled, as shown in Figure 8. A uniform 10×10 mesh of nine-node membrane elements is used. Symmetry boundary conditions are applied on AB (fixed

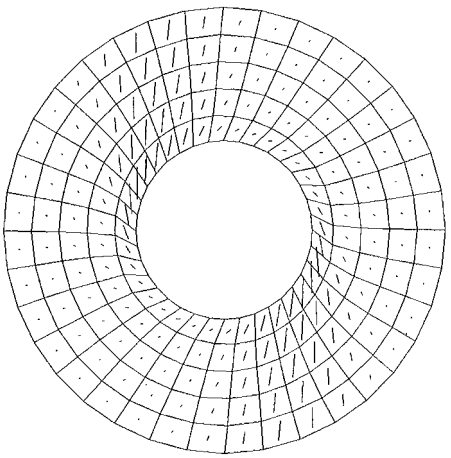

Figure 7. Deformed mesh with principal Cauchy stresses vectors for orthotropic analysis.

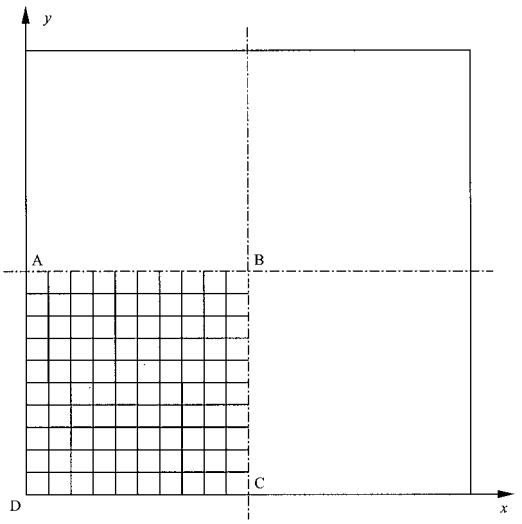

Figure 8. Finite element mesh of one eighth of the airbag.

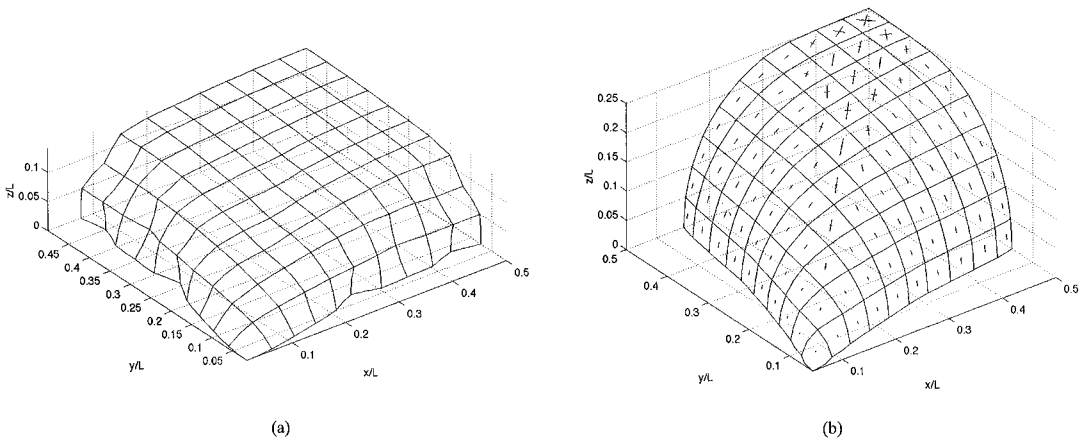

Figure 9. Three-dimensional view of inflated airbag: (a) without wrinkling and (b) with wrinkling (Principal Cauchy vectors are shown).

in y-direction), BC (fixed in x-direction) and CD and AD (fixed in z-direction). This problem is evaluated with and without the membrane wrinkling algorithm.

A three-dimensional view of the inflated airbag without and with the wrinkling algorithm is shown in Figure 9. The principal Cauchy stress vectors with the wrinkling algorithm are shown. The length of the vectors represents the magnitude of the stresses. Regions with one vector are wrinkled, regions with two orthogonal vectors are taut, and regions without vectors are slack.

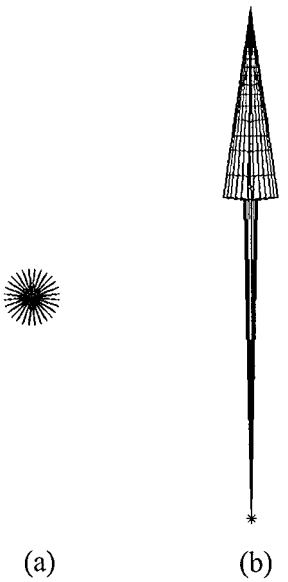

Figure 10. Initial configuration of parachute: (a) top view and (b) side view.

The predicted inflated shapes and stresses without and with the wrinkling algorithm are dramatically different. The maximum in-plane deflection (point C) is 0.144 in with wrinkling and 0.077 in without wrinkling. The maximum transverse deflection (point B) is 0.252 in with wrinkling and 0.1 in without wrinkling. The maximum principal stress at B is about $+4000\,\mathrm{lb/ft^2}$ with wrinkling and $+7500\,\mathrm{lb/ft^2}$ without wrinkling. The predicted solution without the wrinkling algorithm has large regions of high compressive principal stress around the edge with a maximum value of $-20\,000\,\mathrm{lb/ft^2}$. No compressive stresses appear in the results when the wrinkling algorithm is used. Removal of the compressive stress dramatically changes how the structure resists the load, which results in very different inflated shape.

4.4. Inflation of a round parachute

The wrinkling algorithm is implemented in a finite element code that is currently being developed to simulate the dynamics of parachute systems [12]. In this example, the inflation of a round parachute from an initially unstressed and highly folded configuration is evaluated with and without the wrinkling algorithm. The finite element model of the initial configuration is shown in Figure 10. The model is three dimensional and completely unconstrained, and corresponds to a half-scale C-9 parachute consisting of 28 gores, suspension lines, and payload. The gores are initially folded along their centres. The finite element model uses 896 four-node membrane elements and 700 two-node cable elements. Cable elements are used to model the suspension lines, but also run continuously through the canopy to model canopy reinforcement. Typical parachute material properties are used (density $= 0.6\,\mathrm{lb/ft^3}$, Young's modulus $= 4.32\times10^6\,\mathrm{lb/ft^2}$ and Poisson ratio $= 0.3$, thickness $= 0.0001\,\mathrm{ft}$). The model is subject to constant internal pressure (pressure $= 0.1\,\mathrm{lb/ft^2}$) and gravity. The simulation used 6000 time steps with a length of 0.0001 s each. Mass proportional damping was also applied which stabilizes the solution and allows a larger

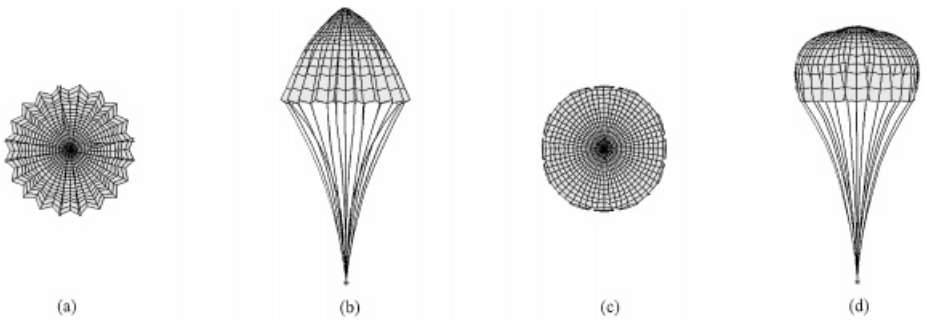

Figure 11. The shape of the parachute during inflation: (a) top view without wrinkling; (b) side view without wrinkling; (c) top view with wrinkling and (d) side view with wrinkling.

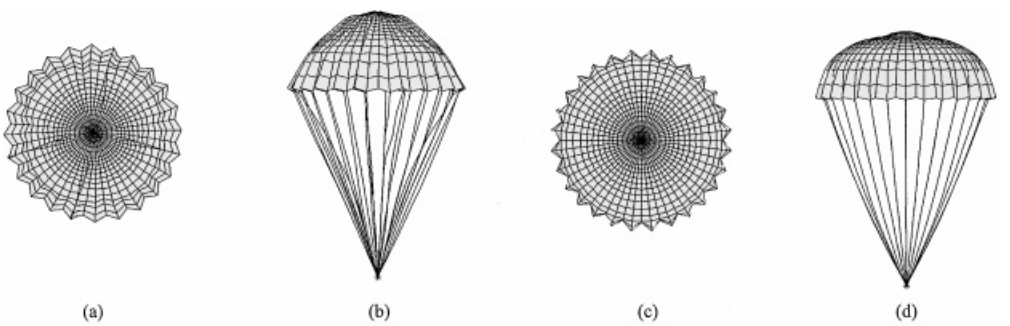

Figure 12. Final inflated shape of parachute: (a) top view without wrinkling; (b) side view without wrinkling; (c) top view with wrinkling and (d) side view with wrinkling.

time step to be used. Lumped mass matrices were used for all elements and were found to result in faster convergence than consistent mass matrices.

Figure 11 shows the top and side views of the parachute during the inflation as predicted without and with the wrinkling algorithm. Figure 12 shows a similar view for the fully inflated shape. The predicted shapes without and with the wrinkling algorithm are dramatically different. Predicted shapes using the wrinkling algorithm are intuitively more correct in appearance. Note that the structure and loading possess complete cyclic symmetry which is not utilized in these three-dimensional simulations. The simulations without wrinkling showed a significant loss of symmetry, whereas the ones with wrinkling did not. The small bump at the canopy vent (Figures 11(d) and 12(d)) was found to be caused by the mass proportional damping which can be eliminated by using a smaller time step [15].

The history of the maximum principal Cauchy stress at a point located at the middle of the gore approximately halfway down the canopy meridian is shown in Figure 13. The predicted stress magnitudes without and with wrinkling are dramatically different. With the wrinkling algorithm, there is never any compressive stress. Without wrinkling, large compressive stress regions exist over much of the history (not shown) which dramatically affect the shape and stress distribution in the canopy.

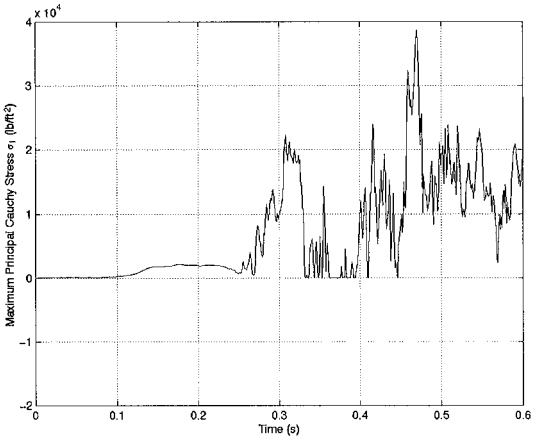

(a)

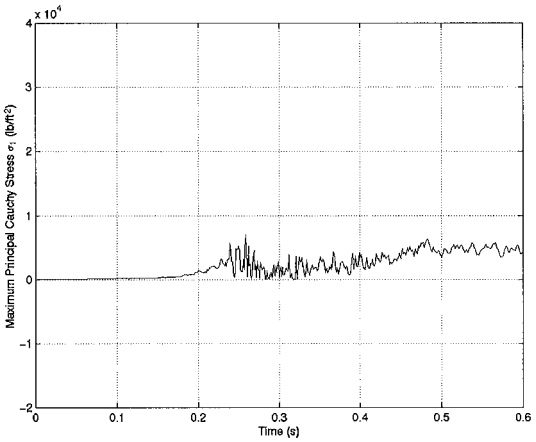

(b)

Figure 13. Maximum principal Cauchy stress histroy around the middle of the meridian: (a) without wrinkling and (b) with wrinkling.

5. CONCLUSIONS

New results were presented for the analysis of wrinkling in curved elastic membranes undergoing large deformation using general curvilinear co-ordinates. A concise continuum theory and finite element formulation was developed which results in explicit expressions for the internal force vector and tangent stiffness matrix.

The new results were implemented in a finite element code and several benchmark problems were performed for validation. Two demonstration problems were also presented. In all these problems, the results obtained with and without the wrinkling algorithm were very different. These problems clearly demonstrate that for membrane structures that cannot carry compression, it is essential to include a wrinkling algorithm in the analysis in order to get realistic results. In general, the use of the wrinkling algorithm was found to increase the number of non-linear iterations compared to

no wrinkling algorithm. The use of lumped mass matrices with the wrinkling algorithm required less iterations than consistent mass matrices.

APPENDIX. FORMULAS FOR PARTIAL DERIVATIVES

Let

$$\mathbf{s}_1 = \cos\theta, \quad \mathbf{s}_2 = \sin\theta, \quad \mathbf{s}_1' = -\sin\theta, \quad \mathbf{s}_2' = \cos\theta \tag{A1}$$

$$N_0^{\tau\upsilon} = \mathbf{s}_\sigma \mathbf{s}_\varsigma C^{\sigma\varsigma\tau\upsilon}, \qquad B_0 = N_0^{\tau\upsilon} E_{\tau\upsilon}, \quad A_0 = N_0^{\tau\upsilon} \mathbf{s}_\tau \mathbf{s}_\upsilon \tag{A2}$$

$$N_1^{\tau\upsilon} = 2\mathbf{s}_\sigma' \mathbf{s}_\varsigma C^{\sigma\varsigma\tau\upsilon}, \qquad B_1 = N_1^{\tau\upsilon} E_{\tau\upsilon}, \quad A_1 = 2N_1^{\tau\upsilon} \mathbf{s}_\tau \mathbf{s}_\upsilon \tag{A3}$$

$$N_2^{\tau\upsilon} = 2(\mathbf{s}_\sigma' \mathbf{s}_\varsigma' - \mathbf{s}_\sigma \mathbf{s}_\varsigma) C^{\sigma\varsigma\tau\upsilon}, \quad B_2 = N_2^{\tau\upsilon} E_{\tau\upsilon}, \quad A_2 = 2N_2^{\tau\upsilon} \mathbf{s}_\tau \mathbf{s}_\upsilon + 4N_1^{\tau\upsilon} \mathbf{s}_\tau' \mathbf{s}_\upsilon \tag{A4}$$

$$A_3 = N_1^{\tau\upsilon} \mathbf{s}_\tau' \mathbf{s}_\upsilon, \quad A_4 = N_2^{\tau\upsilon} \mathbf{s}_\tau' \mathbf{s}_\upsilon \tag{A5}$$

$\partial\theta/\partial u_i^I$ is calculated from

$$\frac{\partial\theta}{\partial u_i^I} = -\frac{Q_1}{P} \tag{A6}$$

where

$$P = N_2^{\alpha\beta} \tilde{E}_{\alpha\beta} - \frac{B_1 + \gamma A_1}{A_0} \frac{A_1}{2} + 2\gamma A_3 \tag{A7}$$

$$Q_1 = N_1^{\alpha\beta} \frac{\partial E_{\alpha\beta}}{\partial u_i^I} - \frac{N_0^{\tau\upsilon}}{A_0} \frac{\partial E_{\tau\upsilon}}{\partial u_i^I} \frac{A_1}{2} \tag{A8}$$

$\partial\tilde{E}_{\alpha\beta}/\partial u_i^I$ is obtained from

$$\frac{\partial \tilde{E}_{\xi\eta}}{\partial u_i^I} = \frac{\partial E_{\xi\eta}}{\partial u_i^I} - \frac{\partial\theta}{\partial u_i^I} \frac{(B_1 + \gamma A_1)}{A_0} \mathbf{s}_\xi \mathbf{s}_\eta - \frac{N_0^{\tau\upsilon}}{A_0} \frac{\partial E_{\tau\upsilon}}{\partial u_i^I} \mathbf{s}_\xi \mathbf{s}_\eta + \gamma \frac{\partial\theta}{\partial u_i^I} (\mathbf{s}_\xi' \mathbf{s}_\eta + \mathbf{s}_\xi \mathbf{s}_\eta') \tag{A9}$$

by substituting the result of $\partial\theta/\partial u_i^I$ (A6) into (A9).

$\partial^2\theta/(\partial u_i^I\, \partial u_j^J)$ is calculated from

$$\frac{\partial^2\theta}{\partial u_i^I\, \partial u_j^J} = -\frac{Q_2}{P} \tag{A10}$$

where

$$\begin{aligned} Q_2 = {} & \frac{\partial^2 E_{\alpha\beta}}{\partial u_i^I\, \partial u_j^J} \left(N_1^{\alpha\beta} - \frac{N_0^{\alpha\beta}}{A_0} \frac{A_1}{2} \right) + \frac{\partial\theta}{\partial u_i^I} \frac{\partial\theta}{\partial u_j^J} \left[\frac{2(B_1 + \gamma A_1)}{A_0} \left(\frac{A_1}{A_0} \frac{A_1}{2} - 2A_3 \right) \right. \\ & \left. - \frac{B_2 + \gamma A_2}{A_0} \frac{A_1}{2} + 2\gamma A_4 \right] + \left(\frac{N_0^{\xi\eta}}{A_0} \frac{A_1}{A_0} \frac{A_1}{2} - \frac{N_1^{\xi\eta}}{A_0} \frac{A_1}{2} - \frac{N_0^{\xi\eta}}{A_0} 2A_3 \right) \\ & \times \left(\frac{\partial\theta}{\partial u_i^I} \frac{\partial E_{\xi\eta}}{\partial u_j^J} + \frac{\partial\theta}{\partial u_j^J} \frac{\partial E_{\xi\eta}}{\partial u_i^I} \right) + N_2^{\alpha\beta} \left(\frac{\partial\theta}{\partial u_i^I} \frac{\partial \tilde{E}_{\alpha\beta}}{\partial u_j^J} + \frac{\partial\theta}{\partial u_j^J} \frac{\partial \tilde{E}_{\alpha\beta}}{\partial u_i^I} \right) \end{aligned} \tag{A11}$$

$\partial^2\tilde{E}_{\alpha\beta}/(\partial u_i^I\,\partial u_j^J)$ is obtained from

$$\begin{aligned}\frac{\partial^2\tilde{E}_{\xi\eta}}{\partial u_i^I\,\partial u_j^J} &= \frac{\partial^2 E_{\xi\eta}}{\partial u_i^I\,\partial u_j^J} - \frac{\partial^2\theta}{\partial u_i^I\,\partial u_j^J}\frac{(B_1+\gamma A_1)}{A_0}\mathbf{s}_\xi\mathbf{s}_\eta + \frac{\partial\theta}{\partial u_i^I}\frac{\partial\theta}{\partial u_j^J}\left[\frac{2(B_1+\gamma A_1)}{A_0}\frac{A_1}{A_0} - \frac{B^{(2)}+\gamma A^{(2)}}{A_0}\right]\mathbf{s}_\xi\mathbf{s}_\eta \\ &+ \left(\frac{N_0^{\tau\upsilon}}{A_0}\frac{A_1}{A_0} - \frac{N_1^{\tau\upsilon}}{A_0}\right)\left(\frac{\partial\theta}{\partial u_i^I}\frac{\partial E_{\tau\upsilon}}{\partial u_j^J} + \frac{\partial\theta}{\partial u_j^J}\frac{\partial E_{\tau\upsilon}}{\partial u_i^I}\right)\mathbf{s}_\xi\mathbf{s}_\eta - \frac{N_0^{\tau\upsilon}}{A_0}\frac{\partial^2 E_{\tau\upsilon}}{\partial u_i^I\,\partial u_j^J}\mathbf{s}_\xi\mathbf{s}_\eta \\ &- \frac{\partial\theta}{\partial u_i^I}\frac{\partial\theta}{\partial u_j^J}\left[2\frac{B_1+\gamma A_1}{A_0}\left(\mathbf{s}'_\xi\mathbf{s}_\eta + \mathbf{s}_\xi\mathbf{s}'_\eta\right)\right] - \frac{N_0^{\tau\upsilon}}{A_0}\left(\mathbf{s}'_\xi\mathbf{s}_\eta + \mathbf{s}_\xi\mathbf{s}'_\eta\right)\left(\frac{\partial\theta}{\partial u_i^I}\frac{\partial E_{\tau\upsilon}}{\partial u_j^J} + \frac{\partial\theta}{\partial u_j^J}\frac{\partial E_{\tau\upsilon}}{\partial u_i^I}\right) \\ &+ \gamma\left[\frac{\partial^2\theta}{\partial u_i^I\,\partial u_j^J}\left(\mathbf{s}'_\xi\mathbf{s}_\eta + \mathbf{s}_\xi\mathbf{s}'_\eta\right) + 2\frac{\partial\theta}{\partial u_i^I}\frac{\partial\theta}{\partial u_j^J}\left(\mathbf{s}'_\xi\mathbf{s}'_\eta - \mathbf{s}_\xi\mathbf{s}_\eta\right)\right] \qquad \text{(A12)}\end{aligned}$$

by substituting the result of $\partial\tilde{E}_{\alpha\beta}/\partial u_i^I$ from (A9) and $\partial^2\theta/(\partial u_i^I\,\partial u_j^J)$ from (A10) into (A15).

ACKNOWLEDGEMENTS

The research described in this paper was supported by the U.S. Army Research Office under grant number DAA04-96-1-0051 to the University of Connecticut and by the U.S. Army Natick RD&E Centre.

REFERENCES

1. Libai A, Simmonds JG. *The Nonlinear Theory of Elastic Shells* (2nd edn). Cambridge University Press: New York, 1998; 276–280, 431–441.
2. Miller RK, Hedgepeth JM, Weingarten VI, Das P, Kahyai S. Finite element analysis of partly wrinkled membranes. *Computers and Structures* 1985; **20**:631–639.
3. Steigmann DJ, Pipkin AC. Wrinkling of pressurized membranes. *ASME Journal of Applied Mechanics* 1989; **56**: 624–628.
4. Wu CH, Canfield TR. Wrinkling in finite plane-stress theory. *Quarterly of Applied Mathematics* 1981; **39**:179–199.
5. Roddeman DG, Drukker J, Oomens DWJ, Janssen JD. The wrinkling of thin membranes: part I—theory. *ASME Journal of Applied Mechanics* 1987; **54**:884–887.
6. Roddeman DG, Drukker J, Oomens DWJ, Janssen JD. The wrinkling of thin membranes: part II—numerical analysis. *ASME Journal of Applied Mechanics* 1987; **54**:888–892.
7. Roddeman DG. Finite element analysis of wrinkling membranes. *Communications in Applied Numerical Methods* 1991; **7**:299–307.
8. Kang S, Im S. Finite element analysis of wrinkling membranes. *ASME Journal of Applied Mechanics* 1997; **64**: 263–269.
9. Press WH, Teukolsky SA, Vetterling WT, Flannery BP. *Numerical Recipes in FORTRAN*: *the Art of Scientific Computing*. Cambridge University Press: New York, 1992; 352–355.
10. Muttin F. A finite element for wrinkled curved elastic membranes and its application to sails. *Communications in Numerical Methods in Engineering* 1996; **12**(11):775–786.
11. Leonard JW. *Tension Structures*. McGraw-Hill: New York, 1988.
12. Accorsi M, Leonard J, Benney R, Stein K. Structural modelling of parachute dynamics. *AIAA Journal* 2000; **38**(1): 139–146.
13. Lu K, Enhanced membrane elements for simulation of parachute dynamics. *PhD Dissertation*, University of Connecticut, August 1999.
14. Contri P, Schrefler B. A geometrically nonlinear finite element analysis of wrinkled membrane surfaces by a no-compression material model. *Communications in Applied Numerical Methods* 1988; **4**:5–15.
15. Accorsi M, Lu K, Leonard J, Benney R, Stein K. Issues in parachute structural modelling: damping and wrinkling. *15th CEAS/AIAA Aerodynamic Decelerator Systems Technology Conference*, AIAA-99-1729, 1999; 193–204.

